Available online at www.sciencedirect.com
ScienceDirect
Journal of Solid State Chemistry 180 (2007) 3485–3492
JOURNAL OF SOLID STATE CHEMISTRY
www.elsevier.com/locate/jssc

Structural features of zinc hydroxyfluoride

H. Serier, M. Gaudon*, A. Demourgues, A. Tressaud

ICMCB, CNRS, Université Bordeaux 1, 87 avenue du Dr. A.Schweitzer, 33608 Pessac Cedex, France

Received 6 June 2007; received in revised form 24 September 2007; accepted 1 October 2007
Available online 13 October 2007

Abstract

Zinc hydroxyfluoride (ZnOHF), obtained by coprecipitation of a zinc salt in aqueous HF, exhibits a variable stoichiometry $Zn(OH)_{2-x}F_x$, where x is tuneable from 0.63 to 0.87 by controlling the pH of the solution. The structure was determined from Rietveld refinements using X-ray powder diffraction data. Crystallizing with the orthorhombic symmetry (SG : $Pna2_1$), the ZnOHF-type structure exhibits two different anionic sites. A bond valence analysis shows that fluorine exclusively occupies the anionic site that has shorter contacts to zinc. This site is split into two partially occupied sites, one corresponding to the position of a fluoride ion and the other to the position of a hydroxide ion. Bond valence calculations show that the split site model gives a more accurate picture of the local coordination of the anions on this site.

Keywords: Zinc; Hydroxyfluoride; Rietveld refinement; Bond valences

1. Introduction

A few studies have been performed [1–4] on basic halides with MOHX chemical formula, where M is a divalent metal (zinc or cadmium) and X is a halogen either chlorine or fluorine. These investigations have dealt with the preparation, the determination of the composition and crystal structure of MOHX compounds. Some of these compounds were analysed by ^{19}F NMR or thermal analysis in order to compare their properties with those of homologous $M(OH)_2$ hydroxide and to deduce the impact of the halogen on the chemical reactivity as well as the thermal stability [2,3].

Zinc hydroxyfluoride (ZnOHF) is generally synthesized by hydrolysis–condensation of zinc fluoride tetrahydrate in water followed by evaporation at 100 °C to dryness. ZnOHF could be also obtained by thermal degradation under air of zinc fluoride (ZnF_2) [4] or, more recently, could be observed on the surface of ZnO films due to a treatment with a NH_4F aqueous solution [5]. Moreover most of the authors considered that F^- and OH^- groups are in equimolar proportion in ZnOHF but no accurate chemical analyses were carried out. Our study shows that it is possible to directly obtain a $Zn(OH)_{2-x}F_x$ compound by coprecipitation of a zinc salt into aqueous HF at various pH and that the amount of fluorine in the compound is tuneable by experimental conditions. Furthermore, the crystal structure of $Zn(OH)_{2-x}F_x$ has been investigated versus the fluorine amount and two different atomic positions for the fluorine and the hydroxyl groups have been proposed by taking account the valence states and the cation–anion bond distances. Then, the local environments of anions have been followed and discussed versus the fluorine content.

1.1. Experimental

1.1.1. Synthesis

$Zn(OH)_{2-x}F_x$ hydroxyfluorides were prepared from zinc chloride ($ZnCl_2$ 98%, Aldrich), hydrofluoric acid (HF 40%, Panreac) and ammonium hydroxide (NH_4OH 98%, Aldrich). A zinc chloride solution was added drop wise into a continuously stirred fluorinated medium to form a white precipitate. The precipitation was carried out at constant pH by simultaneous addition of a NH_4OH solution (commercialized solution diluted by 1/3). After complete addition of the $ZnCl_2$ solution (about 20 mL), the volume is

*Corresponding author.
E-mail address: gaudon@icmcb-bordeaux.cnrs.fr (M. Gaudon).

0022-4596/$ - see front matter © 2007 Elsevier Inc. All rights reserved.
doi:10.1016/j.jssc.2007.10.007

Table 1
Sample names (A1–A3 : F/Zn = 2, A4–A6 : F/Zn = 8), identified phases and fluorine amount present in $Zn(OH)_{2-x}F_x$ compounds with their standard deviation determined via two analytical methods

Sample	pH	Identified phases	Microprobe	F^- electrode
A1	5	ZnF_2/ $ZnF_2 \cdot 2H_2O$	##	##
A2	6	ZnOHF	0.83 ± 0.01	0.91 ± 0.02
A3	7	ZnOHF	0.67 ± 0.03	0.80 ± 0.02
A4	5	No precipitate	##	##
A5	6	ZnOHF	0.79 ± 0.02	##
A6	7	ZnOHF	0.71 ± 0.01	##

adjusted in order to have a final constant fluorine concentration (about 1.2 mol/L). The mixture was still stirred for another 30 min to favour dissolution/growth mechanisms (Ostwald ripening) and the one formation of the 'thermodynamically stable' phase. The white powder was then filtered, washed several times with distilled water and dried at 100 °C in an oven during an hour.

In the precipitation process, two parameters could be adjusted such as the working pH during the addition of zinc solution and the F/Zn molar precursor ratio. With this process, the formation of a white precipitate occurred for $5 \leqslant pH \leqslant 7$ but when the ripening time is increased, a precipitate appears also at pH equal to 4 and 8. The compounds, reported in Table 1, were then synthesized at pH varying from 5 to 7 and for an F/Zn molar ratio equal to 2 (samples A1–A3 with a final $[Zn^{2+}]$ equal to 0.62 M) or 8 (samples A4–A6 with a final $[Zn^{2+}]$ equal to 0.15 M) in order to identify the impact of these parameters on the final chemical composition and on the crystal structure of the compounds.

2. Powder X-ray diffraction (XRD) pattern refinements

XRD patterns were collected using a PANalytical X'Pert MPD PW 3040 with Cu$K\alpha_1$ radiation ($\lambda_1 = 1.540562$ Å) and the measurements were performed with a scan step of 0.02° in the 2θ range from 5° to 130°. The FULLPROF program [6] was used for pattern matching process and structural refinement.

The isotropic profile refinement using the Le Bail method (pattern matching) was performed using the pseudo-Voigt function. In this case, the evolution of the full width at half maximum H versus the Bragg angle θ is provided by the Caglioti law $H^2 = (U_{ins} + U_{obs}) \tan^2\theta + (V_{ins} + V_{obs}) \tan\theta + (W_{ins} + W_{obs})$, where U, V and W are profile parameters and the index *ins* and *obs* correspond to the instrumental contribution (peak broadening contribution linked to the experimental set-up and the diffraction recording mode) and to the observed sample contribution, respectively.

In the refinements, the Thompson–Cox–Hastings pseudo-Voigt function was used to study the broadening related to the sample morphology, i.e. particle size and micro-strains (defects or dislocations). Actually this function enables to dissociate accurately the sample contribution to the instrumental one. This latter, calculated from a LaB_6 reference analysis, can be described by a Gaussian contribution, given by the Caglioti law (U_{ins}, V_{ins} and W_{ins}). For the sample contribution, the relationship between the Gaussian and the Lorentzian parts of H and θ becomes $H_G^2 = (U_{ins} + DST(hkl)^2) \tan^2\theta + V_{ins} \tan\theta + W_{ins} + G/\cos^2\theta$ and $H_L^2 = X \tan\theta + (Y + F(hkl))/\cos\theta$; DST and X being related to the Gaussian and the Lorentzian broadening contributions respectively due to micro-strains, G and Y corresponding to the Gaussian and the Lorentzian contributions respectively due to the crystallite and microdomain size. F(*hkl*) is the anisotropic factor associated to the (*hkl*) orientation.

3. Chemical analyses

An electron probe microanalysis (EPMA) using a CAMECA SX 630 was firstly performed to determine the amount of fluorine and zinc, the hydroxyl content being deduced from the electroneutrality equation. The experiments were carried out with a 20 kV accelerating voltage and a 10 nA probe current (LaB_6). Each pellet was analysed at five different spots in order to determine an average amount and a standard deviation, the analysis depth and the area of each spot being respectively equal to 1 μm and 225 μm^2 (15 μm × 15 μm) in order to avoid surface phenomenon. The calibration was performed with a NaF standard for fluorine and with metallic Zn for zinc.

The fluorine amount was also determined by a fluoride ion-selective electrode calibrated with different diluted solutions of standard NaF (NaF 1 mg/1 mL, Aldrich). The powders were dissolved in an HCl aqueous solution and the pH was then adjusted to 5–6 by addition of NH_4OH. The addition of a TISAB III solution enabled to adjust the ionic strength and to favour the ions diffusion during the measurement (support electrolyte). For each sample, the fluorine amount was deduced from nine measurements (with three standard solutions containing different fluorine concentrations and three TISAB III concentrations) in order to accurately evaluate the average value with the standard deviation.

4. Results and discussion

4.1. Determination of the chemical composition

The XRD analysis of the as-prepared samples, reported in Table 1, shows that for pH values varying from 6 to 7, a pure zinc hydroxyfluoride-type structure (referred with JCPDS n°74–1816) is always obtained. Otherwise for an F/Zn molar ratio equal to 2 (A1–A3), a mixture of ZnF_2 and the corresponding hydrated compound $ZnF_2 \cdot 2H_2O$ appears at pH lower than 6. In the case of an F/Zn ratio

equal to 8 (A4–A6), no precipitation is observed after 30 min for pH $\leqslant$ 5 because of the low zinc concentration.

In the literature [1–4], ZnOHF-type compounds are mainly reported with an equimolar proportion of F and OH groups but without accurate structural analyses. However there is no prevention that the ZnOHF structure corresponds to a compound whose the F/OH molar ratio is different from unity, this ratio being adjusted by the experimental conditions. For instance the pH can have a decisive impact on the fluorine incorporation into the compound because of a competition between OH^- and F^- ions in solution, a low pH involving a higher fluorine concentration.

According to the results of the chemical analyses, with their standard deviation provided in Table 1, the fluorine amount is always lower than 1, the F/OH ratio varying between 0.67(3) and 0.83(1) for the EPMA and between 0.80(2) and 0.91(2) for the fluoride ion-selective electrode. It should be noted that the pH has actually a relevant impact on the fluorine content: the lower the pH, the higher the final fluorine amount. The F/OH ratio in the final compound is directly linked to the F/OH molar ratio in the solution, which remains almost constant when the pH is fixed whatever the F/Zn molar ratio. Consequently the pH appears the most significant parameter to tune the chemical composition of 'ZnOHF' compound.

In the following part, A2 and A3 samples, corresponding respectively to a pH equal to 6 and 7 and to an F/Zn molar ratio equal to 2, will be investigated in more details.

4.2. Crystal structure of zinc hydroxyfluorides

From a structural point of view, ZnOHF crystallizes with an orthorhombic symmetry (SG : $Pna2_1$), derived from the diaspore $\alpha-AlOOH$ (SG : *Pnma*), in which all atomic positions correspond to a general 4*a* position. In this structure exhibiting 4 atoms par cell, zinc cations are located in a distorted octahedral site, whereas anions are three-fold-coordinated to Zn^{2+} ions. The structure provides only one 4*a* cationic site and two 4*a* anionic sites, corresponding to sites 1 and 2, respectively in Fig. 1. In the first one, anions are located at the intersection between two edge-shared octahedra linked to a third octahedron by a corner and in the second site, anions are placed at the boundary of three edge-shared octahedra. The latter exhibits an anion–cation average bond distance longer than for the first site because of stronger Zn–Zn interactions at the origin of a competitive bond.

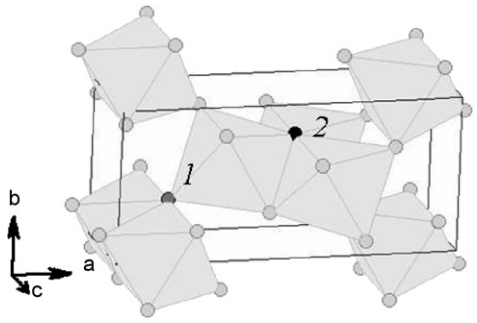

Fig. 1. Representation of ZnOHF unit cell (SG : $Pna2_1$). All anions are represented by spheres with an example of sites 1 and 2.

The impact of the fluorine amount on the lattice parameters was first investigated by performing a pattern matching process using the Le Bail method. An isotropic peak profile function was firstly used to describe the X-ray patterns, but this peak profile function did not bring a good agreement with the experimental data, the reliability factors being reported in Table 2. Indeed, as shown by the pattern enlargement in Fig. 2, some peaks such as those corresponding to the (201) plane are significantly narrower than the other ones such as the (310) plane for example. This anisotropic broadening of the peaks can arise from an 'anisotropic shape' of the crystallites and/or from directional 'micro-strains'. Therefore both types of contributions were taken into account in refinements and the Thompson—Cox–Hastings pseudo-Voigt function was used to fit data and get information about the particles morphology and 'micro-strains'. As the plot of FWHM versus the diffraction angle provided no information about the relevance of each contribution, several orientations were attempted for a needle-platelet model in order to

Table 2
Results of the X-ray diffraction data refinements for samples A2 and A3 using an isotropic model (Caglioti function factors, reliability factors, etc.) and an anisotropic model (Thompson–Cox–Hastings function factors, reliability factors, etc.)

Parameters	A2	A3
Isotropic model		
a (Å)	10.228(1)	10.255(1)
b (Å)	4.7165(6)	4.7177(5)
c (Å)	3.1125(3)	3.1137(3)
V (Å^3)	150.15(5)	150.65(5)
U	0.58(4)	0.49(4)
V	−0.31(3)	−0.29(3)
W	0.077(6)	0.085(6)
χ^2	5.20	4.57
CR_p	13.0	10.9
CR_{wp}	15.4	13.6
Anisotropic model		
a (Å)	10.2276(4)	10.2546(3)
b (Å)	4.7161(2)	4.7175(2)
c (Å)	3.1130(1)	3.1137(1)
V (Å^3)	150.15(2)	150.63(2)
X	0.33(2)	0.21(2)
Y	0.200(8)	0.225(6)
DST	0	0.007(9)
G	0	0.0066(6)
F(010)	−3.0(2)	−3.1(1)
χ^2	4.39	2.92
CR_p	12.4	9.03
CR_{wp}	14.4	11.1

found the anisotropy direction and to improve the pattern matching. Then the highest anisotropy corresponding to the F(010) anisotropic factor and the best conventional reliability factors were noticed for a two-dimensional (2D)-platelet model perpendicular to (010) direction. As one can see on the difference diagram in Fig. 2 and also with the reliability factors reported in Table 2, this anisotropic model enables a slight improvement in the refinements.

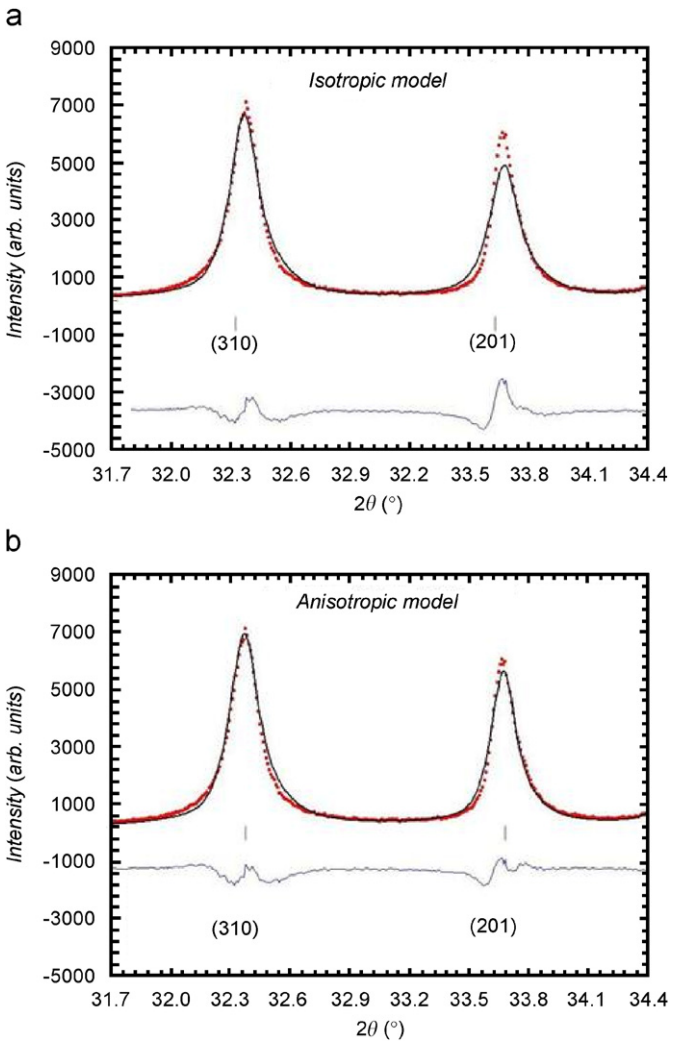

Fig. 2. Effect of anisotropic model on the sample A2 pattern matching for the (310) and (201) planes of ZnOHF-type structure.

As shown in Table 2, micro-strains are negligible compared to the crystallite shape contribution. Then it is possible to schematize shape of the particles, reported in Table 3, from previous refinements. One can notice that the anisotropy is more remarkable for the A2 sample than for the A3 sample but this difference cannot be explained until now even if this could be linked to the fluorine amount.

Concerning the profile refinements of A2 and A3 samples, it can be noticed that the lattice parameters and consequently the lattice volume, increase ($\Delta V/V = 0.3\%$) with decreasing pH values and consequently with the F/OH atomic ratio. This phenomenon can be related to the Zn-OH bond distances that are longer than Zn–F distances.

SEM analyses have been carried out to corroborate the proposed hypotheses concerning the particles shape. In a first step, spherical agglomerates constituted of anisotropic objects getting a particular ordering were observed on SEM pictures, as shown for A2 sample in Fig. 3a. The formation of spherical agglomerates can be explained by the easiness for particles to reorganize in a liquid medium, via van der Waals forces, thus minimizing the total surface energy. Once broken by ultrasonics, the agglomerates reveal the presence of three different particle shapes, represented in the three insets of Fig. 3b. The powders seem to be composed by large isotropic three-dimensional (3D) objects (frame 1), platelet-like particles (frame 2) and needle-like particles (frame 3) even if the former shapes cannot be differentiated by this 2D-technique. This heterogeneity of morphologies allows to explain the difficulty to refine a XRD diagram which corresponds to the result of an average analysis.

In the following part, the Rietveld method was used from both pattern matching models in order to locate atoms. The fluoride and hydroxyl ions (both with 10 electrons) cannot be directly differentiated by XRD because both anionic groups exhibit almost similar structural or atomic form factors. Therefore all structural refinements were arbitrarily performed with the fluorine

Table 3
Particle sizes and anisotropy obtained from the structural refinements (Le Bail method) of samples A2 and A3

	(100) nm	(010) nm	(001) nm
A2	179	28	179
A3	62	23	62

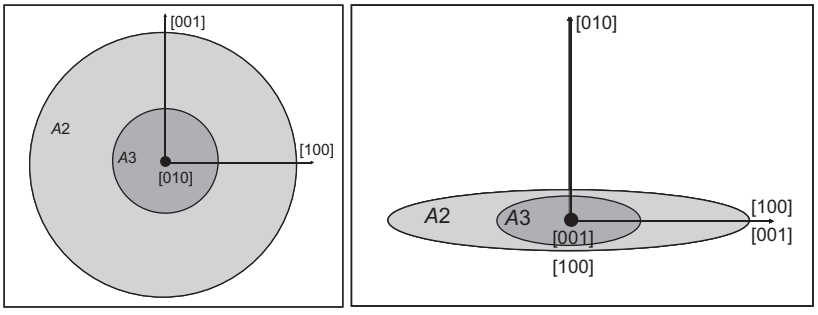

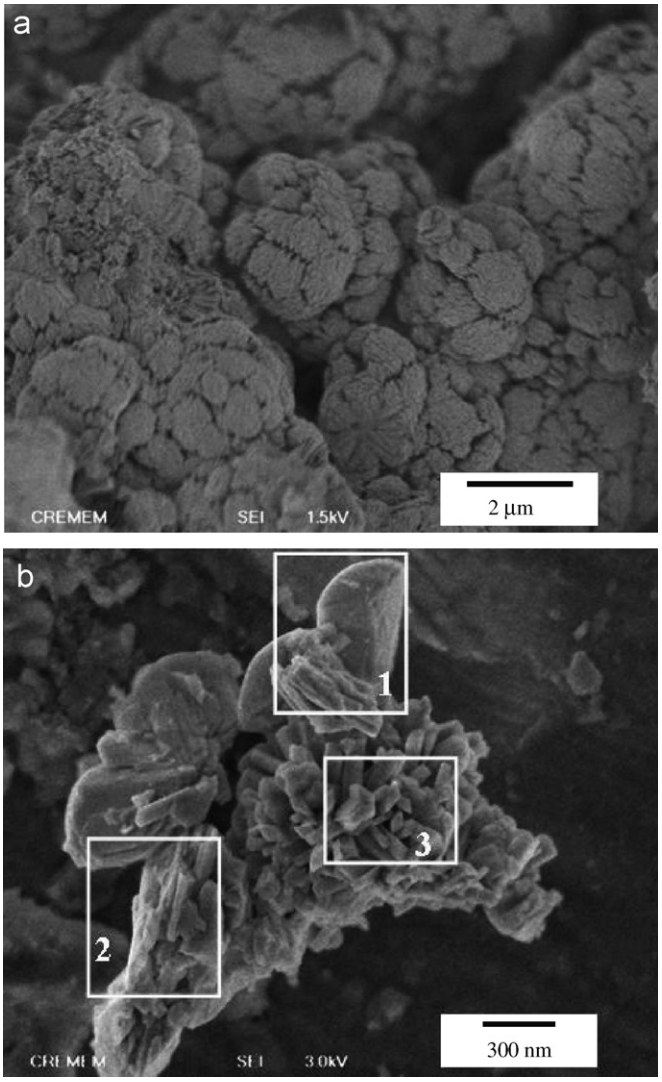

Fig. 3. SEM pictures of sample A2 (a) powder without preliminary preparation, (b) powder dispersed in ethanol by ultrasounds.

ions form factor in the two anionic sites (F1 and F2 corresponding to sites 1 and 2 respectively), the results being reported in Table 6. However, the fluoride and hydroxyl ions can be also compared by analyzing the cation–ligand bond distances that are different for the two groups. A method to follow this difference is to calculate the bond-valence parameters of each cation–ligand bonds. That enables to know if fluorine atoms are randomly distributed on both anionic sites or if fluorine is preferentially set in only one of the two anionic sites.

The bond-valence parameters were calculated with the Brown and Altermatt model [7] $V_i = \Sigma \exp(r_0'\text{-}r_{ij}/B)$, where r_0' is a constant tabulated for several structures and which can be provided in the literature, r_{ij} is the anion–cation bond distances in the considered site and B is a parameter defined by Brown and Altermatt and equal, in our case, to 0.37. For the Zn–O chemical bond the r_0' value is equal to 1.704, as indicated in the literature [7], whereas the r_0' value corresponding to the Zn–F bond has been calculated taking into account the ZnF_2 fluoride reported in the literature [8] and is equal to 1.627. The bond-valence values account for the part of electrons localized on the anionic site; thus, the partial valence provided by this bond, will be a positive partial value for cations ($\delta+$) and a negative value for anions ($\delta-$). This model was used hereafter to calculate the whole valence of each ion, equal to the sum of all partial bonds-valences, in order to evaluate the agreement with the refined bond distances deduced from the XRD data. In the case of a competition between F and OH groups in various sites, the closer the valence value to −1, the higher the probability of the occupation of anionic site. One can notice that if bond distances increase, then the absolute value of valence decrease. Furthermore, the bond valence sum of hydroxyl will be calculated from Zn–O bond distances.

After refinements, whose results are reported in Table 4, the whole valence sum of zinc was firstly calculated for various hypotheses: all fluoride ions are either (i) totally located in site 1 or (ii) totally placed in site 2 or (iii) randomly distributed in both sites. The whole valence sum of zinc is slightly affected by these distributions and therefore that does not enable to conclude on the fluorine position.

Then, in a second step, the whole valence sums for each anion, reported in Table 5, have been calculated for both anionic sites from bond distances, similar to bond distances proposed by Volkova et al. [9]. For both samples, the fluorine bond valence sum diverges significantly from −1, to values near −0.8 (i.e. bond distances are too long) for site 2, whereas it is roughly equal to −1 for the site 1. Moreover, one can note that the hydroxyl valence in site 1 is significantly lower than −1 (equal to −1.15) while is approximately equal to −1 in site 2. It can be thus assumed that fluoride ions are located only on site 1. Since the hydroxyl valence is lower than -1 whereas the fluorine

Table 4
Rietveld refinement results for samples A2 and A3 without site 1 splitting

Atom	*x*	*y*	*z*	*B* (Å^2)
Zn	0.13816(3)	0.0313(8)	0	0.72(8)
	0.1385(1)	*0.0318(4)*	*0*	*0.85(5)*
F1	0.303(1)	0.793(3)	0	1.5(4)
	0.3047(6)	*0.800(1)*	*0*	*2.1(2)*
F2	0.949(1)	0.213(2)	0	0.8(3)
	0.9482(6)	*0.210(1)*	*0*	*1.3(2)*

Parameters	A2	A3
χ^2	5.29	3.38
CR_p	14.0	9.46
CR_{wp}	15.8	11.8
R_B	4.99	3.10
R_F	3.55	2.44

Italics refer to sample A3, whereas normal fonts refer to sample A2 (atomic positions, Debye–Waller values and reliability factors).

Table 5
Global valence parameters of fluorine and hydroxyl groups with or without site 1 splitting and corresponding interatomic distances

	A2	A3
Without site 1 splitting		
Distances (Å)	2.026(12)	2.025(6)
Site 1	2 × 2.075(9)	2 × 2.089(4)
V_F	0.936	0.915
V_{OH}	1.153	1.126
Distances (Å)	2.116(10)	2.125(6)
Site 2	2 × 2.132(7)	2 × 2.125(4)
V_F	0.778	0.781
V_{OH}	0.957	0.962
With site 1 splitting		
Distances (Å)	2.019 (6)	1.974(5)
Site 1-1	2 × 2.046(4)	2 × 2.074(4)
V_F	0.991	0.989
Distances (Å)	2.062(9)	2.100(6)
Site 1-2	2 × 2.143(7)	2 × 2.123(4)
V_{OH}	0.991	0.987
Distances (Å)	2.113(2)	2.126(1)
Site 2	2 × 2.133(1)	2 × 2.123(1)
V_{OH}	0.957	0.964

valence is higher than −1, an adjustment of the bond distances between zinc and anions, i.e. an increase of the zinc–hydroxyl bonds and a decrease of the zinc–fluorine bonds would enable the valences of fluorine and hydroxyl groups to tend to −1.

This last observation leads to consider a splitting of the site 1 into two new positions: one corresponding to fluorine atoms and the other one to hydroxyl atoms. Nevertheless the two created positions, indexed F1-1 and F1-2, were refined from XRD data by considering only the fluorine and the zinc atomic form factors. One can notice that the Fourier transform, provided in Fig. 4, corresponding to the observed XRD data shows already that the anionic site 1 exhibits a slight anisotropy represented by a double arrow. Moreover one should have to point out that the Debye Waller value of the site 1 remains high (1.5–2.1) due to an OH/F disorder whereas the one of the site 2 is close to 1 $Å^2$ (0.8–1.3). Therefore it was consistent to consider a splitting of the former site. Since two new anionic positions were created, two sets of zinc–anion bond distances were deduced for the site 1 with one of the two sets constituted of shorter bonds than the other one, the fluorine atoms corresponding to the smallest distances. The Rietveld refinements were also performed considering different amounts of fluorine ions in site 1, i.e. various occupancies for each newly created position. Because this occupancy directly impacts on the two new atomic positions, this evolution can be discussed considering the whole valence of two anions in their position. The dependence with the fluorine amount in the two compounds of the whole valence of both anions is reported in Fig. 5. The bond

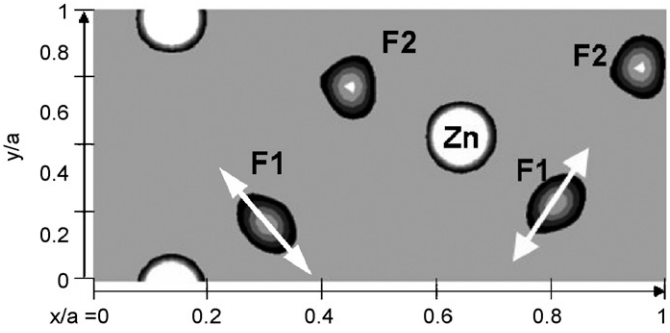

Fig. 4. Fourier map from observed powder X-ray diffraction data of the sample A2.

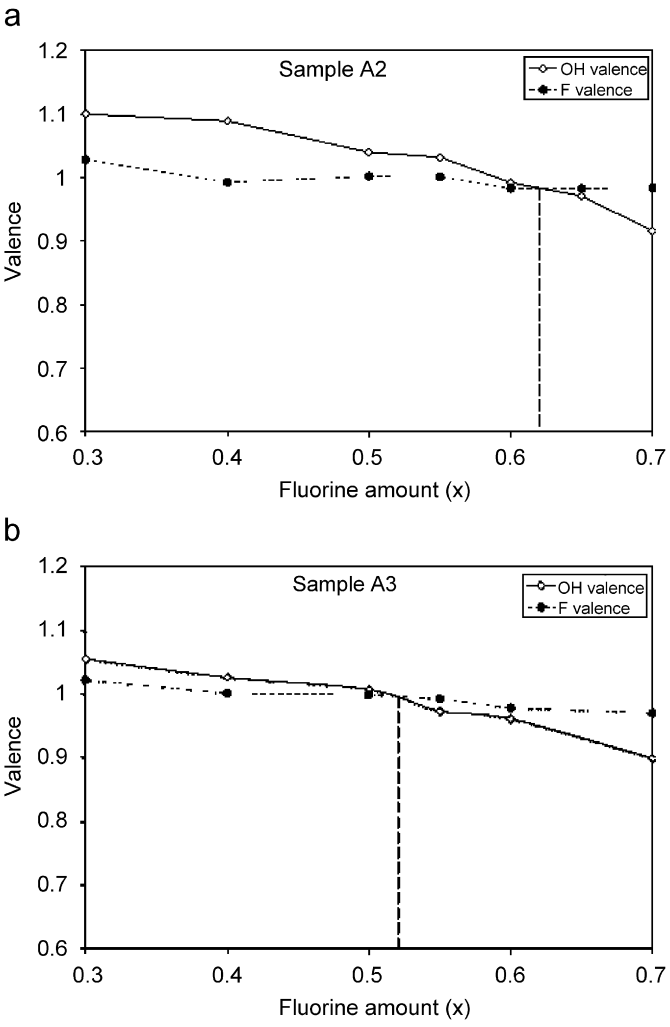

Fig. 5. Variation of fluorine and hydroxyl valences for different rates of each split position for samples A2 and A3.

distances allowing the calculation of anionic valences have been obtained by refining the structure for each concerned fluorine amount. In Fig. 5, one can see that the fluorine valence is nearly constant whereas the hydroxyl valence varies significantly and continuously versus the fluorine content. The fluorine amount deduced from the XRD refinements, corresponding to the intersection of both

Table 6
Rietveld refinement for samples A2 and A3 with site 1 splitting.

Atom	x	y	z	B (Å^2)	Occ.
Zn	0.1382(3)	0.0314(8)	0	0.75(9)	1
	0.1386(1)	*0.0320(4)*	*0*	*0.88(4)*	*1*
F1-1	0.296(4)	0.774(8)	0	0.5(7)	0.62
F$^-$	*0.293(2)*	*0.781(5)*	*0*	*0.7(5)*	*0.52*
F1-2	0.317(6)	0.83(1)	0	2.1(9)	0.38
OH$^-$	*0.319(2)*	*0.824(5)*	*0*	*2.4(7)*	*0.48*
F2	0.949(1)	0.213(2)	0	0.84(3)	1
OH$^-$	*0.9480(5)*	*0.209(1)*	*0*	*1.3(2)*	*1*

Parameters	A2	A3
χ^2	5.24	3.27
CR_p	14.0	9.25
CR_{wp}	15.7	11.6
R_B	4.91	2.48
R_F	3.50	2.22

Italics refer to sample A3 whereas normal letters refer to sample A2. In bold letters are indicated anions present in the corresponding site.

curves that is mean to equal anionic valences and closed to −1, is lower in the A3 sample than in the A2 sample as it was already reported from elemental chemical analyses. Here, for the A2 sample, the best results, i.e. best reliability factors and anionic valences, are obtained when site 1 is split into 62% of fluorine and 38% of hydroxyl group and for A3 sample when the site is split into 52% of fluorine and 48% of hydroxyl groups. The results of final refinements are reported in Table 6. One should have to notice that the reliability factors and also the χ^2 values obtained with appropriated splitting are slightly different from those obtained without splitting because the atomic form factors of hydroxyl and fluorine groups are similar. With as-determined fluorine amount for the A2 and A3 samples, experimental, calculated and difference diffractograms are plotted as illustration in Fig. 6.

Finally, from the x, y, z cartesian coordinates of new F1-1 and F1-2 positions, an axis of splitting can be determined. As it can be seen in Fig. 7, the splitting axis has got its main component along the b-axis, i.e. Δy corresponding to the widest deviation. Moreover as it is underlined in Fig. 7, this splitting of the first anionic site is possible from a steric point of view because it occurs inside an 'empty channel' of the network structure.

5. Conclusion

New zinc hydroxyfluoride $Zn(OH)_{2-x}F_x$, synthesized by coprecipitation, can contain varying amounts of fluorine depending on experimental conditions because of the high flexibility of the structure. Firstly, combining the chemical analyses performed with an electronic microprobe and a fluorine ion-selective electrode, the fluorine content was

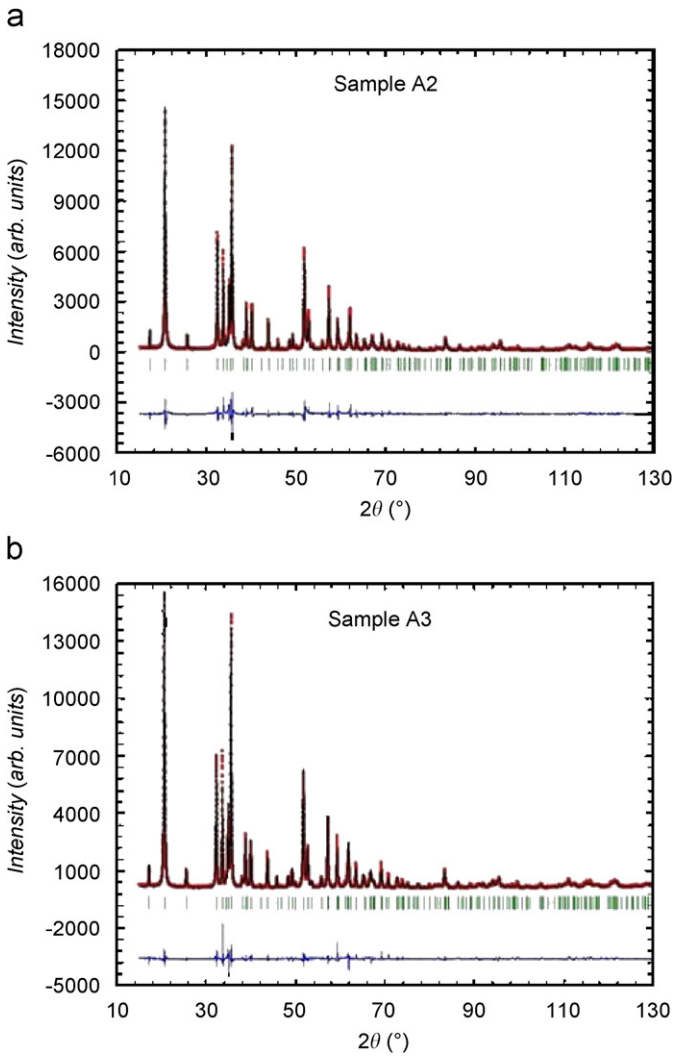

Fig. 6. Powder X-ray diffraction patterns of sample A2 (with 62% fluorine) and sample A3 (with 52% fluorine): experimental data, calculated curve deduced from the anisotropic model with site 1 splitting and difference pattern.

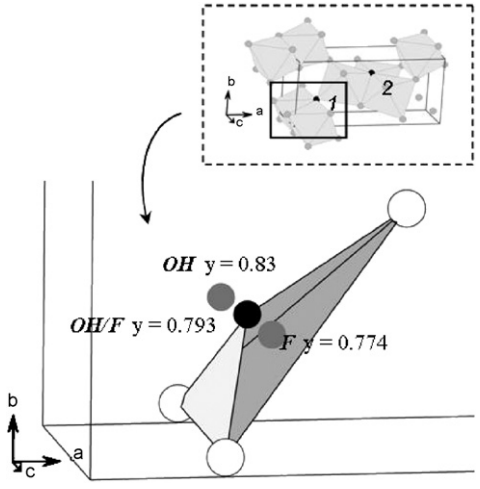

Fig. 7. Representation of the splitting of site 1 (black sphere) into two positions (grey spheres) corresponding respectively to the presence of hydroxyl or fluoride ions.

determined. The fluorine content is always lower than 1 and can be tuned by varying the pH from pH 5 to 7. At pH 6, a compound whose chemical formula is $Zn(OH)_{1.17}F_{0.83}$ is obtained, whereas at pH 7, the chemical composition becomes $Zn(OH)_{1.33}F_{0.67}$.

The synthesized compounds crystallize with orthorhombic symmetry (SG : $Pna2_1$) with all ions in only one Wyckoff position 4*a*. The structure exhibits two anionic sites. Based on the bond distances obtained from powder diffraction refinements, bond valence calculations indicate that the fluoride ions are located exclusively in the smaller anion site. In order to differentiate the anion site preferences, the smaller anion site was split in two newly created positions, each one corresponding to an anionic group (F^- or OH^-). The occupancies of created positions are dependent on the chemical composition and the evolution of anionic valences with the fluorine amount was investigated. An optimal fluorine content for which the refinement leads to correct anionic valences was also determined. The bond valence analysis allowed a possible distinction between two anionic groups, having the same number of electrons and almost the same X-ray scattering factor. This analysis can be achieved because of significantly different cation-anion distances for each anion site.

Finally, concerning others types of metal hydroxyfluorides, one should have to point out that in the case of CdOHF compound whose structure derived from the rutile structure has been determined by single crystal analysis [10], the two different anionic positions (SG : $P2_12_12_1$, 4*a* Wyckoff positions) give rise to almost identical bond distances (2.27 Å). This is also the case of InF_2OH whose the framework derives from the ReO_3-type and where In-F/OH bond distances are almost identical and close to 2.09 Å. In these compounds, because of the increase of the polarizability of cations in the case of Cd^{2+} and In^{3+}, the presence of fluorine or hydroxyl groups in the vicinity of cations does not strongly affect the interatomic distances and thus F and OH specific positions can not be distinguished. Conversely, in HgOHF [11] and CuOHF [12] compounds, an OH/F ordering was found by single crystal analysis.

Acknowledgments

The authors wish to thank E. Sellier, research engineer at the CREMEM, for SEM analyses.

References

[1] W. Feitknecht, Helv. Chim. Acta 26 (1953) 2196.
[2] O.K. Srivastava, E.A. Secco, Can. J. Chem. 45 (1967) 579.
[3] O.K. Srivastava, E.A. Secco, Can. J. Chem. 45 (1967) 585.
[4] M. Nierlich, P. Charpin, P.M.C.R. Herpin, Acad. Sci. Série C: Sci. Chim. 1–3 (1973) 276.
[5] S. Yamabi, H. Imai, Trans. Mater. Res. Soc. Jpn. 28 (2003) 329.
[6] J. Rodriguez-Carvajal, Abstracts of the Satellite Meeting on Powder Diffraction of the XV Congress of the IUCr (1990) 127.
[7] I.D. Bown, D. Altermatt, Acta Crystallogr. B 41 (1985) 244.
[8] N.J. O'Toole, V.A. Streltsov, Acta Crystallogr. B 57 (2001) 128.
[9] L.M. Volkova, L.V. Samarets, S.A. Plishchuk, et al., Kristallografiya 23 (1978) 951.
[10] C. Stålhandske, Acta Crystallogr. B 35 (1979) 2184.
[11] C. Stålhandske, Acta Crystallogr. B 35 (1979) 949.
[12] G. Giester, E.Z. Libowitzky, Kristallogr 218 (2003) 351.